

Nanocrystalline Ti Films Deposited by Modulated Pulsed Power Magnetron Sputtering

Yang Chao, Jiang Bailing, Wang Di, Huang Bei, Dong Dan

Xi'an University of Technology, Xi'an 710048, China

Abstract: Modulated pulsed power magnetron sputtering (MPPMS) has the ability to control the ionization rate, energy and quantity of deposited particles through adjusting the pulsed intensity and duration, thus modifying the nucleation and growth process of the thin film. Nanocrystalline Ti films were deposited using MPPMS technique in a closed field unbalanced magnetron sputtering (CFUBMS) system under different peak target power densities of the strong-ionized period (P_d). The modulated pulse power (MPP) was employed to modify the P_d by varying the pulse lengths and the average target powers. The results show that the nanocrystalline Ti film with a grain size of 11 nm exhibits a dense microstructure and a smooth surface (roughness of 11 nm) when the P_d is $0.86 \text{ kW}\cdot\text{cm}^{-2}$. The improved properties of the as-prepared Ti film were also discussed.

Key words: nanocrystalline; Ti film; modulated pulsed power magnetron sputtering; peak target power density

Nowadays, nanocrystalline Ti film is a potential candidate for the application in aerospace engineering, medical instruments, optical and microelectronic fields due to its superior mechanical strength, well thermal stability, high wear resistance and intrinsic biocompatibility^[1-3]. Nanocrystalline Ti film is commonly fabricated using traditional direct current magnetron sputtering (dcMS) technique, which is a well-established physical vapor deposition technique for preparing metallic or metallic compound thin film at low substrate temperature. And the multi-layer gradient or compound films with smooth surface can be deposited on the substrates by multiple targets of different materials and precise control of target current in the dcMS process^[4]. Thus, dcMS is widely employed in manufacturing semi-conductive and optical thin film^[5]. However, the film fabricated by dcMS always exhibits porous microstructure and poor film-substrate adhesion^[6] due to the shadowing effect^[7] and low mobility of the adatoms^[8] during the deposition process. Therefore, the formation of nanocrystalline Ti film with dense microstructure, smooth surface, and well functional properties is an urgent problem to be solved.

The structure and properties of thin films can be effectively modified by suitably controlling the energy and ion flux of

deposited particles in the deposition process. When deposited particles possess high ionization rate and high energy (5~20 eV), a dense film with favorable film-substrate adhesion can be achieved^[9]. In addition, the high kinetic energy transferred from the deposited ions to the adatoms will increase the mobility and diffusivity of adatoms, thus generating a large number of nucleation sites and decreasing the grain size of the film. The ion flux and energy of deposited particles are strongly dependent on the sputtering technique and target power. Recently, the application of developed modulated pulsed power magnetron sputtering (MPPMS) technology is proposed^[10], which can produce high peak power density (up to $0.5\sim 1.5 \text{ kW}\cdot\text{cm}^{-2}$), almost 100 times higher than that of traditional dcMS technique. Therefore, high ionization rate of the deposited particles can be obtained. Moreover, the pulse of the MPPMS avoids overheating of the target material even with such a high power density^[11], and reduces the formation of droplets and macroparticles on the film surface^[12]. It should be pointed out that a typical modulated pulse power (MPP) mode consists of two stages in one pulse. The first step is the weak-ionized period, in which low power is loaded on the target to ignite the plasma. Then, the pulse enters the strong-ionized period with high power. In addition, the

Received date: November 27, 2018

Corresponding author: Yang Chao, Ph. D., Lecturer, School of Materials Science and Engineering, Xi'an University of Technology, Xi'an 710048, P. R. China, Tel: 0086-29-82312812, E-mail: yangchao0107@sina.com

Copyright © 2019, Northwest Institute for Nonferrous Metal Research. Published by Science Press. All rights reserved.

MPPMS technique can arbitrarily modify the pulsed intensity and duration to obtain different plasma properties and stable discharge for different target materials.

In this study, nanocrystalline Ti films were deposited using MPPMS technique with different peak target power densities of the strong-ionized period (P_d) in a closed field unbalanced magnetron sputtering (CFUBMS) system. The P_d is affected by pulse length and average target power, which can regulate the intrinsic properties of deposited particles (energy, quantity, ionization rate, etc) to improve the microstructure and then enhance the mechanical and tribological properties of nanocrystalline Ti films. In addition, the correlations between the properties of deposited particles generated at different P_d and the resultant microstructure and properties of nanocrystalline Ti films were investigated systematically.

1 Experiment

A MPP power source was applied to deposit Ti films from a metal Ti target (99.95%) in a CFUBMS system, in which four vertically unbalanced magnetrons were equipped in the chamber wall. And circular Ti target with a diameter of 100 mm and a thickness of 7 mm was used. The effective sputter area of target enclosed in the sputter track was 37 cm², which was used to calculate the target power density. The substrates (silicon wafer and 304# stainless steel) were ultrasonically cleaned in acetone and alcohol for 15 min separately, and then installed into the sample holder. The substrate was parallel to the target surface, and the distance between the target and the substrate was 130 mm. The schematic diagram is presented in Fig.1.

A base pressure less than 3.0×10^{-4} Pa was achieved prior to deposition. As for all depositions, the working pressure was 0.5 Pa and the Ar flow rate was 60 mL/min. At the first deposition, the substrate was cleaned by Ar⁺ plasma etching with a pulsed DC substrate bias voltage of -400 V (40 kHz and 98% duty cycle, Pinnacle Plus, Advanced Energy Inc.)

for 15 min to remove the surface contamination. In the following Ti film deposition, the Ti target was powered by a MPP generator with the substrate bias voltage of -60 V (40 kHz and 98% duty cycle). MPP generated different P_d values by varying the pulse lengths (D_s) and the average target powers (P_{as}) in the strong-ionized period. The pulse frequency of MPP was fixed at 50 Hz. The deposition parameter is presented in Table 1.

The crystal structure of the Ti film was characterized by X-ray diffractometry (XRD-7000S, Shimadzu Limited Corp.) using Cu K α radiation (45 kV, 40 mA) in the range of 30°~80° with 0.02° increments. The thickness and microstructure of the Ti film were observed by field-emission scanning electron microscopy (Ultra-55, Zeiss) and transmission electron microscopy (JEM-3010, JEOL Ltd). The hardness and Young's modulus of the Ti film were measured using a nanoindenter (G200, Agilent Technologies) equipped with a Berkovich diamond indenter. The calculation was proposed by Oliver and Pharr's method from the load-displacement curve with a 10% coating thickness as the indentation depth [11]. The residual stress of Ti film was measured by an IC flatness and a wafer stress analyzer (BGS-6341, BJOE technology). Film-substrate adhesion was evaluated by microscratch tester (WS-2005, ZKKH Instruments Inc.) at an applied load of 0~60 N. The scratch track and film failure morphology were observed by an optical microscope (GX71, OLYMPUS Inc.). The wear resistance of the Ti film was evaluated by a ball-on-disk microtribometer (UMT Tribolab, Bruker Corp.) in an ambient atmosphere (relative humidity 20 ± 1 RH%, temperature 21 ± 1 °C) by sliding against a 1 mm WC-Co ball at a velocity of 25 mm·s⁻¹ for 150 m. The load applied on the sample surface was 2 N, which was controlled by a load suspension system. After the wear test, the wear track was examined by a laser scanning confocal microscopy (LEXT-OLS4000, OLYMPUS Inc.) to measure the wear rate.

Table 1 Deposition parameter of MPPMS Ti films

Sample	f / Hz	d / %	D_w / ms	D_s / ms	P_{aw} / kW	P_{as} / kW	P_{ps} / kW	S / cm ²	P_d / kW·cm ⁻²	I_{ps} / A	V_{ps} / V	T_d / min	I_s / A	T_s / °C	V_a / nm·min ⁻¹	V_s / nm·min ⁻¹
A	50	80	8	8	0.3	2.2	5.5	37	0.15	10.0	550	75	0.03	135	143	358
B	50	70	8	6	0.3	2.2	7.3	37	0.20	13.3	554	75	0.07	147	123	410
C	50	60	8	4	0.3	2.2	11.0	37	0.30	19.5	562	75	0.15	151	99	495
D	50	50	8	2	0.3	2.2	22.0	37	0.60	37.8	583	75	0.23	153	76	761
E	50	50	8	2	0.3	3.2	32.0	37	0.86	50.0	640	60	0.35	181	81	811

Note: f -pulse frequency, d -duty cycle of pulse power, D_w -pulse length of weak-ionized period, D_s -pulse length of strong-ionized period, P_{aw} -average target power of weak-ionized period, P_{as} -average target power of strong-ionized period, P_{ps} -peak target power of strong-ionized period, S -area of sputter track, P_d -peak target power density of strong-ionized period, I_{ps} -peak target current of strong-ionized period, V_{ps} -peak target voltage of strong-ionized period, T_d -deposition time, I_s -substrate bias current, T_s -substrate temperature, V_a -average deposition rate, V_s -instantaneous deposition rate

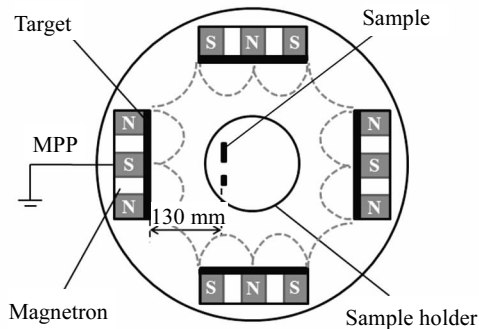


Fig.1 Schematic of the CFUBMS system and the substrate position from the top view

2 Results and Discussion

2.1 Ionization rate and deposition rate

Fig.2 shows the thickness ratio and the average deposition rate (film thickness/deposition time) of samples. The thickness ratio refers to the ratio between the film thickness on the front and back of the substrate. A small value of thickness ratio is an indicator of high ionization rate of deposited particles, because only the ion can be deposited onto the back of the substrate by the negative bias voltage. As shown in Fig.2, the thickness ratios of sample D and E are smaller than those of other samples, suggesting that a higher ionization rate of deposited particles is obtained under the high P_d condition. Moreover, the average deposition rate of sample A to D decreases almost linearly as the P_d increases from $0.15 \text{ kW}\cdot\text{cm}^{-2}$ to $0.60 \text{ kW}\cdot\text{cm}^{-2}$. When P_d increases from $0.6 \text{ kW}\cdot\text{cm}^{-2}$ to $0.86 \text{ kW}\cdot\text{cm}^{-2}$, the average deposition rate is improved slightly (sample D to E). Although the sample D and E have lower average deposition rates than other samples, they exhibit higher instantaneous deposition rates (film thickness/ D_s , Table 1) in the strong-ionized period due to the low D_s .

The decrease in pulse length and the increase in average target power can achieve high P_d in the deposition process. With the increase of P_d , the enhanced ion bombardment not only transmits high energy to the target but also induces structural defects with high resistance on the target surface. The target surface temperature increases significantly due to the heat accumulation from ion bombardment and Joule-heating^[13] in the target material. When the microarea temperature on the target surface exceeds the critical level of thermal emission, a large number of atoms and electrons with high kinetic energy can be emitted from the cathode target. Consequently, a larger number of deposited ions can be created by the high probability of ionization collisions between the deposited atoms and energetic electrons^[14, 15]. Thus, the sample D and E exhibit lower thickness ratios than other samples. However, because the ion can be attracted back toward

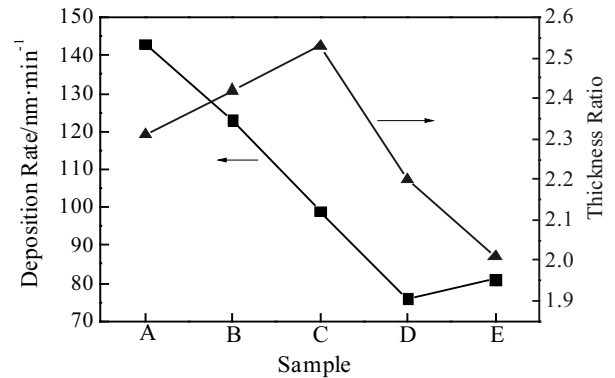


Fig.2 Deposition rate and thickness ratio of samples

the target and be captured by the high negative potential of the cathode, the average deposition rate of sample A to D begins to fall under the same average target power condition. In addition, it is known that increasing average target power will enhance the deposition rate of the film^[16]. Therefore, the average deposition rate of sample E is slightly higher than that of sample D.

2.2 Microstructure

The intrinsic characteristics of deposited particles under the same substrate bias voltage condition significantly affect the microstructure and properties of deposited Ti films. Fig.3 shows the XRD patterns of samples. All samples exhibit a hexagonal closed packed (hcp) Ti structure with (100), (002), (101), (102), (103) and (112) reflections based on JCPDS card 44-1294#. The (002) diffraction peak of sample A to E first increases and then sharply decreases in intensity, and its full width at half maximum (FWHM) exhibit an increasing trend. The FWHM of (002) peak was measured using Jade analysis software. The grain sizes of sample A to E were calculated from the (002) diffraction peak to be 20, 20, 16, 11 and 11 nm, respectively, according to Scherrer's equation^[17, 18].

In order to further investigate the microstructure of Ti films, the high-resolution TEM observations were carried out. As shown in Fig.4a, sample A has a nanoscale crystalline structure (grain size of 20~30 nm), while the selected area electron diffraction (SAED) pattern reveals discontinuous hcp rings with (100), (002) and (101) reflections. However, it is interesting that nanocrystallines (grain size of 5~10 nm) with a random orientation are dispersed in an amorphous matrix of sample E (Fig.4b). The existence of amorphous zone was further analyzed by the SAED pattern, as shown in the inset of Fig.4b. It is known that the broad and diffusive rings in the SAED pattern suggest a typical amorphous structure with nanoparticle composites^[19].

The nucleation process of the thin film is mainly affected by the deposited particle properties, substrate temperature, and deposition rate^[20]. The high ionization rate of deposited particles can be obtained by the MPPMS technique at high P_d , and

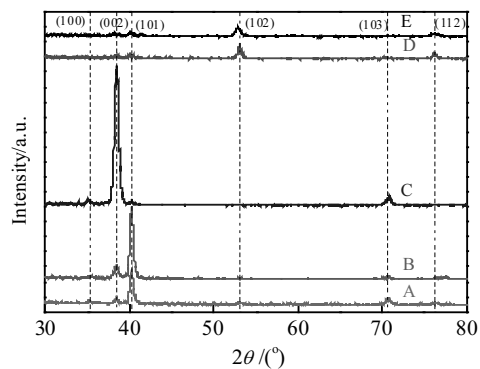


Fig.3 XRD patterns of samples

then a large number of ions are accelerated onto the substrate by negative bias voltage with high kinetic energy. This kinetic energy transferred from the ion to the adatom on the substrate surface will increase the adatom mobility, thereby generating a large number of nucleation sites and decreasing the grain size. The substrate temperature will be enhanced by increasing the P_d (Table 1), which improves the adatom mobility and diffusivity but reduces undercooling of phase transformation. As a result, the critical radius of nucleation is increased and the nucleation number is decreased. Thus, an appropriate substrate temperature is significant to promote the nucleation of the film. It is noted that the substrate temperature can be controlled by the MPPMS technique at different target power densities. In addition, the high instantaneous deposition rate in the transient strong-ionized period under high P_d condition can reduce the critical radius of nucleation and increase nucleation number. Therefore, the nucleation rate increases with the increase of P_d due to the predominant effect of high kinetic energy of deposited particles and the high instantaneous deposition rate, while the nucleation rate changes little when the P_d is higher than $0.6 \text{ kW}\cdot\text{cm}^{-2}$ because of the increase of the substrate temperature. Consequently, the grain size firstly decreases and then remains with increasing the P_d .

Another important feature is a preferred orientation of the films. As shown in Fig.3, sample A and B exhibit a strong (101) preferred orientation, which gradually changes to (002) in sample C. And sample D and E show a (102) preferred orientation. The transition of the preferred orientation is dependent on the competition between strain energy and surface energy during nucleation^[21]. When the substrate temperature or target power improves, the increase of deposited ionic energy will raise the surface mobility of adatoms. Because adatoms possess higher mobility, they are able to select the lowest surface energy plane ((101) for hcp) as the preferred orientation. Thus the sample A and B exhibit (101) preferred orientation. The thermal stress induced in the Ti film deposited at higher substrate temperature may contribute to the modification of (002) preferred orientation, which is the lowest strain energy plane. So the preferred orientation of sample C changes from

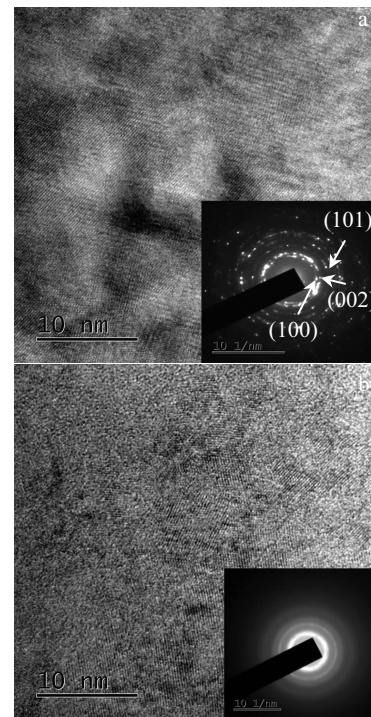


Fig.4 High-resolution TEM images and SAED patterns of sample A (a) and sample E (b)

(101) to (002). Nonetheless, sample D and E show the (102) preferred orientation, because the high instantaneous deposition rate restrains the movement of adatoms on the substrate surface.

Fig.5 shows the surface and cross-sectional SEM micrographs of samples. In order to clearly observe the cross-sectional morphology of the Ti film, different magnifications were selected in SEM observation. Sample A exhibits a branched and porous structure. Sample B to E show large columnar structures throughout the film, and the number of voids/gaps between the columnar structures gradually decreases. Moreover, the columnar structure vertical to the Si substrate cannot be observed in the cross-sectional SEM images, and the width of the columnar structure increases firstly and then decreases. The columnar structure of sample E becomes uniform and dense, and its width decreases to less than 100 nm. In addition, the surface roughness of sample A to E is 80, 58, 24, 16 and 11 nm, respectively, measured by the atomic force microscope (Table 2).

The small ionization rate of deposited particles and the low substrate temperature can be achieved by the low P_d , and they are not capable of providing sufficient accelerated deposition process and ion bombardment onto the substrate surface. Therefore, the adatom is difficult to diffuse on the substrate surface. As a result, the island formation mode is preferred during the film growth process according to Thornton's microstructure classification^[22]. Thus, the morphology of branched/fibrous structure with some voids of the Ti film is

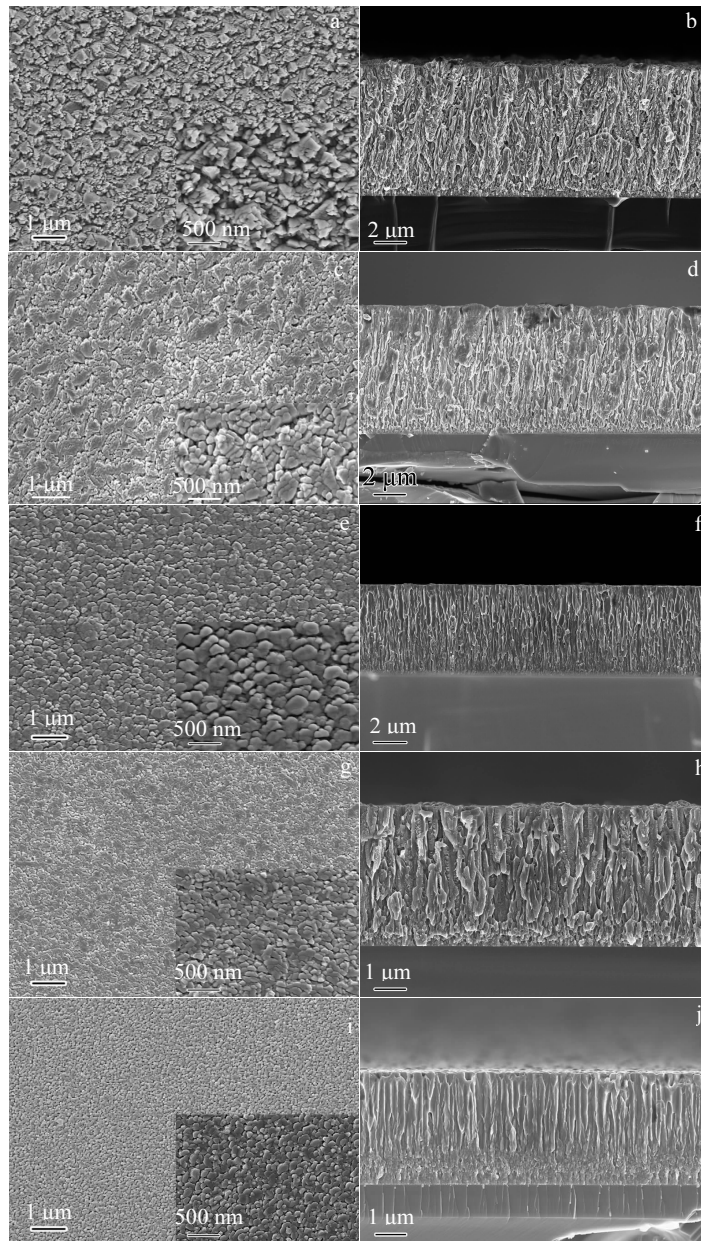


Fig.5 SEM images of sample A (a, b), sample B (c, d), sample C (e, f), sample D (g, h), and sample E (i, j)

formed (Fig.5b). Increasing P_d can increase the mobility of adatoms on the substrate surface considerably, resulting in the transition of the film growth mode from an island formation mode to a layer-plus-island mode, and giving rise to the formation of a columnar structure. Meanwhile, the compactness and width of the columnar structure can be gradually increased (Fig.5c~5f). In addition, the higher instantaneous deposition rate in the film growth process can increase nucleation sites and restrain adatom diffusion on the substrate surface, which is beneficial for decreasing the width of the columnar structure (Fig.5g~5j).

2.3 Mechanical and tribological properties

The mechanical and tribological properties of samples are

summarized in Table 2. The H/E ratio (hardness/Young's modulus, resistance against elastic strain to failure) was evaluated as an important and valuable parameter for tribological coating performance. A higher H/E ratio of coatings is expected to allow the redistribution of the applied load over a large area to delay the failure of the film^[23]. Sample A has the lowest hardness of 1.2 GPa and Young's modulus of 74.1 GPa, resulting in a low H/E ratio of 0.017. The hardness, Young's modulus and H/E ratio are gradually increased to 5.6 GPa, 150.4 GPa and 0.035, respectively, from sample A to E.

The hardness and H/E ratio are influenced by the microstructure, such as grain size^[24, 25], compressive stress, phase segregation^[26], element substitution^[27], compactness^[28] and microstructure

Table 2 Mechanical and tribological properties of samples

Sample	Grain size/nm	Residual stress/GPa	Roughness/nm	Hardness/GPa	Young's modulus/GPa	H/E	L_c/N	COF	Wear rate / $\times 10^{-12}$ $m^3 \cdot N^{-1} \cdot m^{-1}$
A	20	0.5	80	1.2	74.1	0.017	1.3	0.83	4.13
B	20	0.5	58	2.0	94.5	0.021	1.8	0.79	2.33
C	16	0.7	24	3.4	130.4	0.026	2.8	0.75	2.29
D	11	0.3	16	3.7	132.6	0.028	6.5	0.72	1.73
E	11	0.2	11	5.6	150.4	0.035	7.5	0.51	0.26

amorphous phase^[29]. Based on the XRD, XPS, and SEM studies, the grain size and compactness are the main factors considered in this research. The enhanced hardness, Young's modulus and H/E ratio of sample D and E can be closely related to the grain boundary hardening by Hall-Petch relationship^[30] with decreasing the grain size, the compact microstructure, and the intense ion bombardment on the growing film under high P_d condition.

The film-substrate adhesion is evaluated by the critical load (L_c) in microscratch test. L_c is the instant applied load when the film firstly cracks, chips or delaminates^[31]. Scratch track images are presented in Fig.6, which shows the critical film failure events. The first cracking and chipping of all samples within the track occur at the low L_c (inset of Fig.6), and L_c of sample A to E slightly increases from 1.3 N to 7.5 N (Table 2). In addition, sample A and B show the massive film delamination at the edge of the scratch track (Fig.6a and 6b). Both sample D and E have no delamination at the edge of the track until the load increases to 60 N (Fig.6d and 6e).

The film-substrate adhesion is primarily influenced by the residual stress^[32], substrate current (I_s)^[33] and film thickness^[34]. It should be noted that the low L_c for all samples is related to the

presence of residual tensile stress in the present study. Because the residual tensile stress in the film can be reduced by the relatively higher substrate temperature^[35], the heating device will be added in MPPMS deposition process in our subsequent study, in order to decrease the residual stress and enhance the film-substrate adhesion. Generally, the high I_s will enhance the film adhesion, because it not only produces a dense film but also enhances the ion bombardment onto the substrate surface during the deposition. Sample E has the highest I_s due to the accelerated atom ionization under the condition of high P_d (as shown in Table 1), resulting in a good film-substrate adhesion. Besides, increasing the film thickness can also improve the film-substrate adhesion. Therefore, in this study, the residual stress and the I_s are predominant factors affecting the film-substrate adhesion.

The steady friction coefficient (COF) and wear rate of samples against a WC-Co ball were measured through the ball-on-disk test, shown in Fig.7. Sample A exhibits a high COF value of 0.83 and a high wear rate of $4.13 \times 10^{-12} m^3 \cdot N^{-1} \cdot m^{-1}$, which result in a high roughness (80 nm) and low hardness (1.2 GPa). A gradual decrease in both the COF and wear rate is observed from sample A to E, and the sample E exhibits the

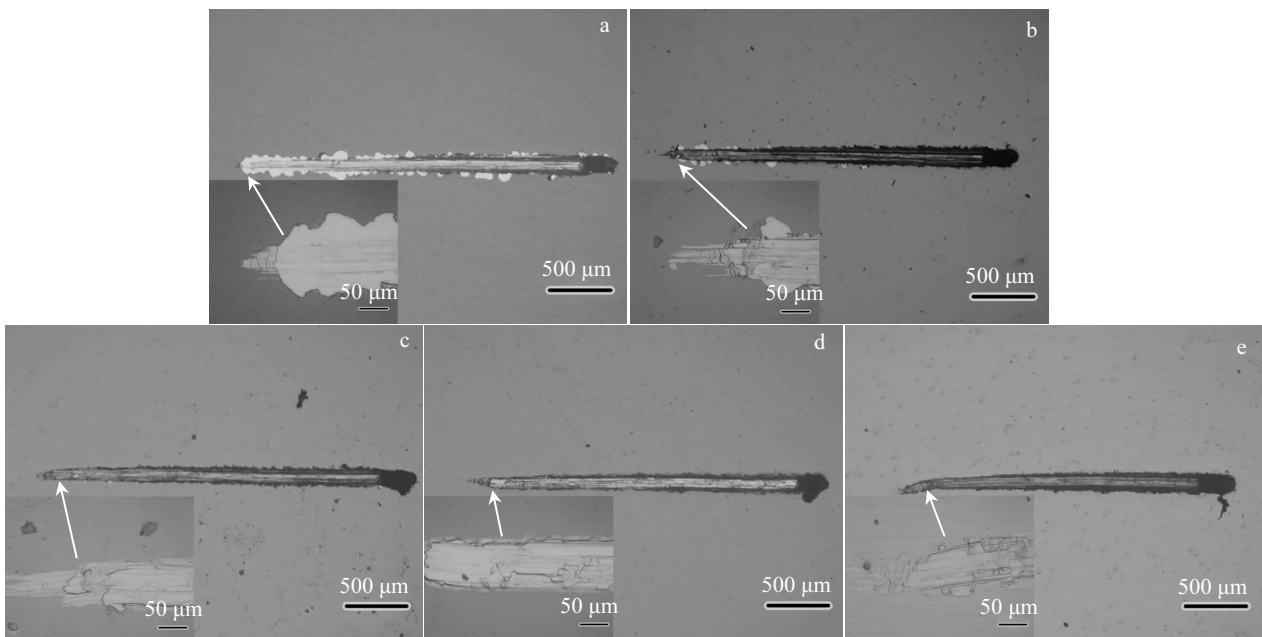


Fig.6 Scratch track morphologies of samples: (a) sample A, (b) sample B, (c) sample C, (d) sample D, and (e) sample E

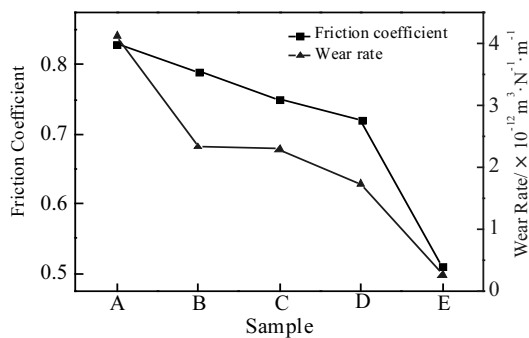


Fig.7 Friction coefficient and wear rate of samples

minimum COF of 0.51 and wear rate of $0.26 \times 10^{-12} \text{ m}^3 \cdot \text{N}^{-1} \cdot \text{m}^{-1}$. These results demonstrate that sample E has better wear resistance than other samples. The improvement of wear resistance is mainly attributed to the improved film compactness, decreased grain size and smooth surface resulting from the enhanced adatom mobility and ion bombardment from the intense plasma under the high P_d condition.

3 Conclusions

1) When the P_d increases from 0.15 to $0.86 \text{ kW} \cdot \text{cm}^{-2}$ by decreasing the pulse width and increasing the average target power, all Ti films exhibit typical hcp nanostructure. The grain size of nanocrystalline Ti films gradually decreases from 20 nm to 11 nm, and the surface roughness is monotonically reduced from 80 nm to 11 nm.

2) The mechanical and tribological properties of nanocrystalline Ti films also vary as a function of P_d . The maximum hardness of 5.6 GPa and an H/E ratio of 0.035 are obtained for the Ti film with P_d of $0.86 \text{ kW} \cdot \text{cm}^{-2}$. The wear resistance of the Ti film is also improved (low COF of 0.51 and low wear rate of $0.26 \times 10^{-12} \text{ m}^3 \cdot \text{N}^{-1} \cdot \text{m}^{-1}$).

References

- Jeyachandran Y L, Karunakaran B, Narayandass S K et al. *Materials Science and Engineering*[J], 2006, 431(1): 277
- Boyer R R. *Materials Science and Engineering*[J], 1996, 213(1-2): 103
- Textor M, Sittig C, Frauchiger V et al. *Titanium in Medicine*[M]. Heidelberg: Springer-Verlag, 2001: 172
- Li J X, Zhang H Q, Fan A et al. *Surface and Coatings Technology*[J], 2016, 294: 30
- Kelly P J, Arnell R D. *Vacuum*[J], 2000, 56(3): 159
- Lin J L, Moore J J, Sproul W D et al. *Surface and Coatings Technology*[J], 2010, 204(14): 2230
- Mukherjee S, Gall D. *Thin Solid Films*[J], 2013, 527: 158
- Lin J L, Moore J J, Sproul W D et al. *Surface and Coatings Technology*[J], 2009, 203(24): 3676
- Petrov I, Barna P B, Hultman L et al. *Journal of Vacuum Science and Technology A*[J], 2003, 21(5): 117
- Lin J L, Moore J J, Sproul W D et al. *Thin Solid Films*[J], 2009, 518(5): 1566
- Pharr G M, Oliver W C. *MRS Bulletin*[J], 1992, 7: 28
- Martin P J, Netterfield R P, Bendavid A et al. *Surface and Coatings Technology*[J], 1992, 54-55(9): 136
- Liu T J. *Engineering Fracture Mechanics*[J], 2014, 123: 2
- Yang C, Jiang B L, Liu Z et al. *Thin Solid Films*[J], 2015, 597: 117
- Yang C, Jiang B L, Feng L et al. *Acta Metallurgica Sinica*[J], 2015, 51(12): 1523
- Posadowski W M. *Thin Solid Films*[J], 2001, 392(2): 201
- Cullity B D, Stock S R. *Elements of X-Ray Diffraction*[M]. London: Prentice-Hall Inc, 2001: 167
- Jenkin R, Snyder R L. *Introduction to X-Ray Diffractometry*[M]. New York: John Wiley and Sons Inc., 1996: 89
- Chen A Y, Bu Y, Tang Y T et al. *Thin Solid Films*[J], 2015, 574: 71
- Tian M B, Li Z C. *Thin Film Technologies and Materials*[M]. Beijing: Tsinghua University Press, 2011: 135
- Chawla V, Jayaganthan R, Chawla A R et al. *Materials Chemistry Physics*[J], 2008, 111(2-3): 414
- Thornton J A. *Journal of Vacuum Science and Technology*[J], 1974, 11: 666
- Matthews A, Franklin S, Holmberg K. *Journal of Physics D: Applied Physics*[J], 2007, 40(18): 5463
- Sergueeva A V, Stolyarov V V, Valiev R Z et al. *Scripta Materialia*[J], 2001, 45(7): 747
- Wang Y M, Ott R T, Buuren T V et al. *Physics Review*[J], 2012, 85(1): 120
- Zhang Y J, Yang Y Z, Zhai Y H et al. *Applied Surface Science*[J], 2012, 258(18): 6897
- Zhang P, Cai Z H, Xiong W Q. *Surface and Coatings Technology*[J], 2007, 201(15): 6819
- Choi S R, Park I W, Kim S H et al. *Thin Solid Films*[J], 2004, 447(4): 371
- Chawla V, Jayaganthan R, Chandra R. *Surface and Coatings Technology*[J], 2010, 204(9-10): 1582
- Nia N S, Savall C, Creus J et al. *Materials Science and Engineering*[J], 2016, 678: 204
- Stallard J, Poulat S, Teer D G. *Tribology International*[J], 2006, 39(2): 159
- Lin J L, Moore J J, Mishra B et al. *Surface and Coatings Technology*[J], 2008, 202(8): 1418
- Laing K, Hampshire J, Teer D. *Surface and Coatings Technology*[J], 1999, 112(1-3): 177
- Heinke W, Leylan A, Matthews A et al. *Thin Solid films*[J], 1995, 270(1): 431
- Inamdar S, Ramudu M, Raja M M. *Journal of Magnetism and Magnetic Materials*[J], 2016, 418: 175

调制脉冲磁控溅射峰值靶功率密度对纯 Ti 镀层沉积行为的影响

杨 超, 蒋百灵, 王 迪, 黄 蓓, 董 丹

(西安理工大学, 陕西 西安 710048)

摘 要: 调制脉冲磁控溅射可通过改变强、弱离化阶段的脉冲强度和占空比等电场参量, 大幅调控镀料粒子的离化率、沉积能量和数量, 实现对沉积镀层形核与生长过程的精确把控。在非平衡闭合磁场条件下, 采用调制脉冲磁控溅射技术, 通过对其强离化脉冲阶段的脉冲宽度和靶功率进行调控获得持续增大的峰值靶功率密度, 并在此条件下制备多组纯 Ti 镀层, 对其微观形貌和力学性能进行了检测分析。结果表明, 当强离化脉冲阶段的峰值靶功率密度由 $0.15 \text{ kW}\cdot\text{cm}^{-2}$ 持续增大至 $0.86 \text{ kW}\cdot\text{cm}^{-2}$ 时, 所制备的纯 Ti 镀层具有 11 nm 的平均晶粒尺寸, 且较其他峰值靶功率密度条件下的制备镀层具有更为致密的组织结构、平整的表面质量 (表面粗糙度 R_a 为 11 nm) 和良好的力学性能。

关键词: 纳米晶; Ti镀层; 调制脉冲磁控溅射; 峰值靶功率密度

作者简介: 杨 超, 男, 1987 年生, 博士, 讲师, 西安理工大学材料科学与工程学院, 陕西 西安 710048, 电话: 029-82312812, E-mail: yangchao0107@sina.com